Supporting Information

Halpern-Manners et al. 10.1073/pnas.1003146107

SI Text

Direct Current Imaging. Direct imaging experiments were performed using Paravision 4.0 and Topspin 1.3 on a 7.05-T Oxford Instruments magnet using a Bruker AVANCE 300 spectrometer. Images were taken with a Bruker MIC 300S1/AS microimaging probe.

The imaging sequence (Fig. S1) consists of a spin-lock module and simultaneous pulsed current preceding acquisition of each line of k space. After rotation of the magnetization into the transverse plane (Fig. S1*A*), the spin lock was applied with intensity resonant with the frequency of a simultaneously applied current pulse (Fig. S1*B*). Following this interval, the M_y component was stored along $\hat{z}$ (Fig. S1*C*), and slice-selective spin-echo imaging was used (Fig. S1*D*). Variations on the spin lock and storage pulse are described within the main text. A two-step phase cycle of the $\pi/2$ pulses and the spin lock was employed to cancel out effects of any residual transverse magnetization after the spin lock.

Photographs of the single and double loop phantoms are shown in Fig. S2 *A* and *B*, respectively. The wire loops sit near the bottom of a 10-mm tube, each with ∼6.5-mm diameter. In the double-loop phantom, the two loops are spaced ∼6.5 mm from each other along the axial dimension. The single-loop phantom has a red circular plastic spacer placed above the solution to aid in centering the current source. Since insulated wire was used, there was no electrical contact with the solution. Current pulses were produced using DS345 (Stanford Research Systems) and 3314A (Hewlett-Packard) function generators synchronized via transistor-transistor logic (TTL) input triggered within the pulse sequence. TTL-triggered multitone signals were generated using a National Instruments USB-6215 DAQ and SignalExpress 3.0. For experiments involving very small current signals, precalibrated attenuators (Mini-Circuits) were used to output the desired voltage.

Loop Field Simulation. Simulations of the magnetic field generated by a simple current loop were performed in Comsol 3.5, using the ac/dc module. The model system consisted of an 8-mm diameter cylinder surrounding the current-carrying "loop," which was modeled as a torus of 28-gauge copper with 6.5-mm loop diameter. Appropriate current density (to model the experiments at 1.5 mV) was determined by connecting a 2-Ω resistor in series with the single-loop phantom and measuring the corresponding voltage drop for a number of signal amplitudes in order to find the current. A map of the axial magnetic flux density within the loop (in T) is shown in Fig. S3, which shows a magnitude of several hundred nanotesla in the central region of the loop. This is consistent with our Fourier analysis, especially given the nonideal nature of our loop phantom (caused by mild deviations from circularity and the transition to the leads running above the loop).

Remote Current Imaging. Remote experiments were performed using VnmrJ on an Oxford Instruments 7.05-T wide-bore magnet and a Varian imaging console. Excitation, spin lock, and storage pulses were performed with a 40-mm Varian volume imaging probe, while gradients were applied using a Varian triple-axis gradient system producing up to 100 G/cm on all three axes. The detection probe was a custom-built microcoil probe connected to the capillary tubing via commercially available connectors (Upchurch Scientific). Water flowed through the system at a constant pressure of ∼10 psi, driven by a nitrogen gas ballast system and regulated by a proportional control system (Omega Engineering).

The remote detection experiment consists of spatially separated encoding and detection steps. The pulse sequence, shown in Fig. S4, begins with an excitation into the transverse plane, which can be made slice selective by the simultaneous application of a refocused gradient along $\hat{z}$ during shaped sinc excitation and storage pulses. Once the magnetization has reached the transverse plane, a collinear spin lock is applied along with a synchronously triggered current pulse to generate the resonant effect. Bipolar velocity-compensated phase encoding is performed along two axes, followed by a storage pulse to return the encoded magnetization components to the longitudinal axis for travel to the detection coil. The stored magnetization is read off stroboscopically within the microcoil by a series of $\pi/2$ pulses, yielding an additional time-of-flight dimension. Phase contrast was generated by comparison with a control image where TTL triggering of the current burst had been disabled. Current and control experiments were interleaved with respect to collection of points in k space. A four-step phase cycle of the storage pulse and receiver phase was employed to store both components of encoded magnetization and to remove artifacts caused by excitation of spins outside the encoding region. Images were taken with 45×45 resolution, with no signal averaging beyond the phase cycle.

Data Processing. Data were processed using Matlab 7.7.0 (Mathworks). For clarity in displaying the 2D current loop images, voxels outside of the sample volume were suppressed by creating a mask from the control image in which voxels with signal intensity lower than a specified percentage of the maximum voxel intensity were set to zero. Three-dimensional images were apodized with Gaussian functions along all three dimensions, and contours plotted at saturation levels of 30%, 50%, 70%, and 90%. In order to generate the field map, the frequency spectrum in each voxel was calculated by Fourier transformation of the oscillating signal after subtracting a best-fit exponential curve in order to eliminate the peak at zero frequency due to relaxation-based decay. The field strength was then calculated by determining the weighted mean of the frequency spectrum. The remote image data were zero-filled by a factor of 2 and apodized along both phase encoding dimensions. The direct dimension of each time-of-flight acquisition was Fourier transformed and then summed across the peak prior to 2D Fourier transformation of the phase encoding dimensions. Phase images were plotted by masking out voxels with intensity less than the maximum intensity multiplied by a cutoff value and determining the relative phase of each voxel between the current image and the control.

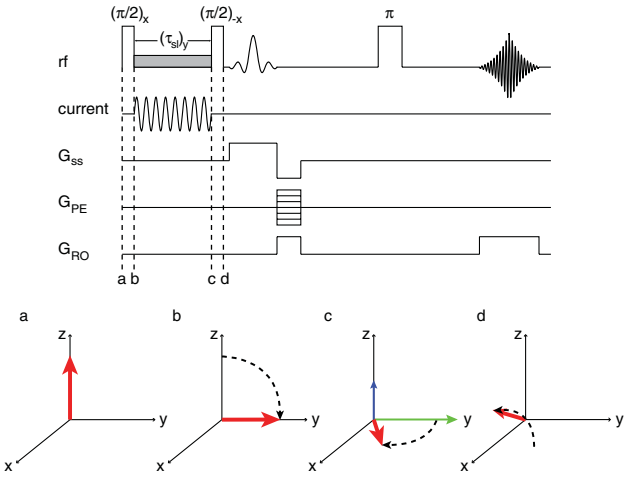

Fig. S1. Conventional spin-echo imaging sequence combined with preceding spin-lock module, application of current, and storage pulse. Corresponding vector diagrams of the magnetization in the doubly rotating frame are shown below, with the spin lock indicated in green, the audio-frequency magnetic field in blue, and the magnetization in red. The initial magnetization aligned along the static field (*A*) is flipped into the transverse plane by a $\pi/2_x$ pulse (*B*), where it proceeds to rotate around the audio field for a time τ_{sl} during application of the resonant spin lock (*C*). Afterward, a second $\pi/2_{-x}$ pulse projects and stores the *y* magnetization along $\hat{z}$ (*D*) in preparation for the imaging sequence.

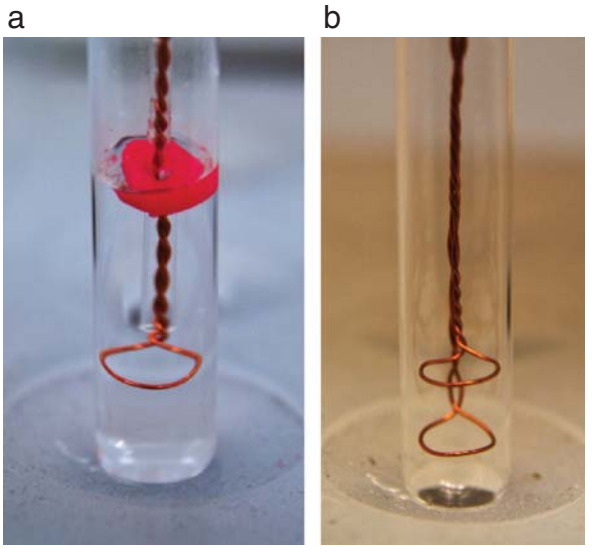

Fig. S2. Single (*A*) and double (*B*) current loop phantoms. Loops were ~6.5 mm in diameter, with ~6.5-mm spacing between loops in the double loop phantom.

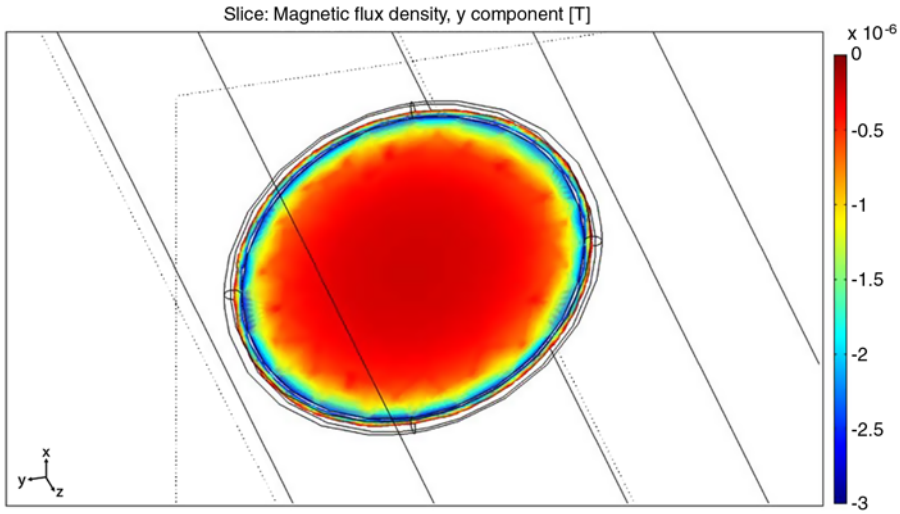

Fig. S3. Simulated magnetic flux density (in T) within a circular current loop of 6.5-mm diameter. The simulation was performed using Comsol 3.5, with parameters appropriate to an imaging experiment with 1.5-mV current.

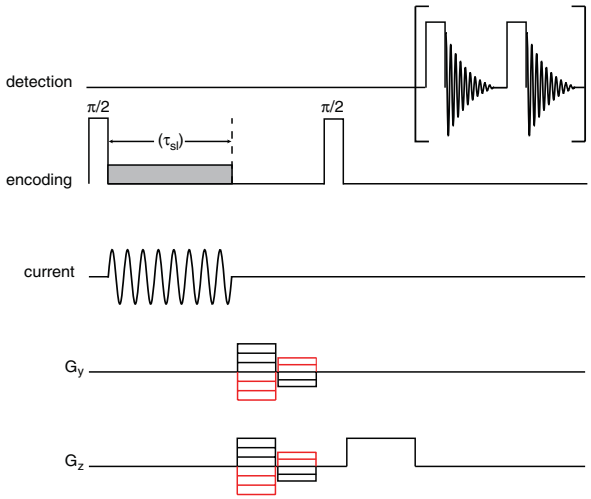

Fig. S4. Remotely detected current imaging sequence. Initial excitation of magnetization into the transverse plane is followed by concurrent application of the oscillatory current pulse and resonant spin lock to generate additional phase in fluid flowing through the current-carrying solenoid. Bipolar velocity-compensated phase encoding gradients are applied along two axes and a second $\pi/2$ pulse stores the encoded magnetization along $\hat{z}$ for transportation to the microcoil (any residual transverse magnetization is destroyed by a crush gradient along $\hat{z}$). The stored magnetization is read off stroboscopically with a series of $\pi/2$ pulses, yielding additional time-of-flight information.